Tuning spin transport across two-dimensional organometallic junctions

Shuanglong Liu,[1,2] Yun-Peng Wang,[1,2] Xiangguo Li,[1,2] James N. Fry,[1] and Hai-Ping Cheng[1,2,*]

[1]*Department of Physics, University of Florida, Gainesville, Florida 32611, USA*
[2]*Quantum Theory Project, University of Florida, Gainesville, Florida 32611, USA*

We study via first-principles modeling and simulation two-dimensional spintronic junctions made of metal-organic frameworks consisting of two Mn-phthalocyanine ferromagnetic metal leads and semiconducting Ni-phthalocyanine channels of various lengths. These systems exhibit a large tunneling magnetoresistance ratio; the transmission functions of such junctions can be tuned using gate voltage by three orders of magnitude. We find that the origin of this drastic change lies in the orbital alignment and hybridization between the leads and the center electronic states. With physical insight into the observed on-off phenomenon, we predict a gate-controlled spin current switch based on two-dimensional crystallines and offer general guidelines for designing spin junctions using 2D materials.

I. INTRODUCTION

To prepare for the future post-Moore era, new and robust functional materials are needed. One candidate is an ultrathin channel transistor that utilizes a two-dimensional (2D) material between different gates [1]. Atomically thin channel materials help mitigate short-channel effects of a transistor, resolving one of the major issues in minimizing electronic devices [2]. Among various 2D materials [3], the organometallic sheet is distinguished by its chemical versatility and tunable electronic structure [4–8]. Another advantage of organometallic electronic devices lies in the seamless contact formed between different organometallic sheets with the same organic framework.

The 2D metal phthalocyanine MPc, where M is a transition metal atom, is an atomically thin organometallic crystal, first synthesized by Abel *et al.* [9,10]. The growth of MPc can be extended to semiconducting surfaces, according to the same authors, which allows electronic devices to be made. An MPc system consists of an organic framework and uniformly distributed metal atoms. Covalent bonds between neighboring unit cells stabilize the atomic structure. Previous theoretical studies showed that the electronic and magnetic properties of MPc can be tuned by changing the embedded transition metal species; specifically, for $M = $ Mn and $M = $ Ni, manganese phthalocyanine (MnPc) and nickel phthalocyanine (NiPc) sheets were predicted to be a ferromagnetic half-metal and a nonmagnetic semiconductor, respectively [11].

In this paper, inspired by experimental feasibility, we study a two-dimensional junction in which semiconducting NiPc sheets are sandwiched between metallic MnPc leads. We find a significant gate dependence of charge transport, and analyze in detail its physical origins. We investigate junctions in different magnetic configurations and evaluate the tunneling magnetoresistance of the junctions. Finally, we discuss the dependence of charge transport properties on the junction length and the validity of theoretical treatments. A number of technical issues are presented in the appendixes.

II. METHOD

Our study is based on density functional theory [12,13] as implemented in the VASP [14,15] and SIESTA [16] computational packages. VASP, in conjunction with projector-augmented-wave (PAW) potential and the Perdew-Burke-Ernzerhof (PBE) functional [17], is used to relax atomic structures, with an energy cutoff of 450 eV and a force tolerance of 0.01 eV/Å. SIESTA is used to calculate the transport properties of MnPc-NiPc-MnPc junctions. In this practice, a double-zeta plus polarization (DZP) basis set and PBE GGA exchange-correlation energy functional [18] are adopted. $1 \times 10 \times 1$ and $1 \times 100 \times 1$ Monkhorst-Pack k grids [19] are set for self-consistent and transmission calculations, respectively. The convergence tolerance is set to 1×10^{-4} eV for energy and to 5×10^{-4} for the probability density matrix. When a gate voltage is applied to the junction, the effective screening medium (ESM) method is used to enforce the boundary conditions for the Hartree potential [20,21]. Transmission coefficients are calculated by the Fisher-Lee relation, which expresses Green's functions in the tight-binding formalism [22]. Finally, we utilize an in-house code to solve the Boltzmann equation when estimating the resistance of the junction [23,24].

III. RESULTS

A. Geometry of the junction

A 2D NiPc sheet is a nonmagnetic semiconductor with a band gap of about 0.49 eV. In contrast, a 2D MnPc sheet is a ferromagnetic half-metal, with an energy gap of 0.33 eV for spin-down electrons. With spin up being the majority, two energy bands cross the Fermi energy. The band structures of MnPc and NiPc are shown in Fig. 10 of Appendix A. The chemical formulas of MnPc and NiPc unit cells are
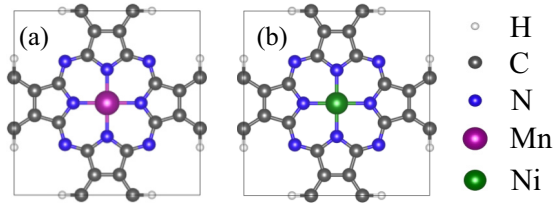
*hping@ufl.edu

FIG. 1. Unit cell of (a) MnPc and (b) NiPc. Neighboring unit cells are bonded covalently. Each unit cell contains one transition metal atom.

$C_{20}H_4N_8Mn$ and $C_{20}H_4N_8Ni$, differing only in the embedded transition metal atom. As shown in Fig. 1, MnPc and NiPc share the same organic framework. According to our calculations, the lattice constants of MnPc and NiPc are 10.66 and 10.56 Å (or a lattice mismatch of just 0.9%), the two can be seamlessly joined together to form a heterostructure. In subsequent calculations, we use the MnPc lattice constant for modeling MnPc-NiPc-MnPc junctions. This choice does not influence the electronic structure of NiPc, as shown in Fig. 11 of Appendix B. The atomic structure of the junction in the y-z plane is shown in Fig. 2. The junction is periodically repeated to $\pm\infty$ in the y direction and charge transport is along the z direction. The two vertical lines mark the boundaries between the center region and the two leads. As can be seen in the figure, three unit cells of MnPc are treated as a screening layer on each side. Our tests show that the boundary between the lead and the center region is bulk-like, indicating the adequacy of the length of the screening layers. The blue arrows on each side indicate the direction of the local magnetization of MnPc. If the arrows are in the same (opposite) orientation, the junction is said to be in the parallel (antiparallel) magnetic configuration.

B. Effects of gate voltage

The major finding from our investigation is an on-off change of state in charge transport. We thus can tune the transport properties of the MnPc-NiPc-MnPc junction by applying a gate voltage. To mimic experimental conditions, both leads and the center region are under a common voltage, which is simulated using the ESM method [20]. With a finite gate voltage, both leads share a common chemical potential, while that of the electrode is different; consequently, the junction becomes charged. A positive (negative) net charge corresponds to hole (electron) doping. We calculate the transmission at the Fermi energy for the MnPc-NiPc-MnPc junction in the parallel magnetic configuration with different charge carrier densities. Results from a scattering center with five NiPc cells are plotted in Fig. 3. There are two important features

seen in this figure. First, the transmission is mostly from spin majority; the minority spin has nearly zero transmission, which makes the junction a spin filter. We will return to discuss the magnetism later. Second, the transmission is small when the carrier density is low, but in the case of hole doping, the transmission suddenly increases when the carrier density is between $3-6 \times 10^{12}$ cm^{-2} and continues to rise as the carrier density increases. The magnitude of transmission changes by three orders of magnitude on crossing the threshold, indicating a *off-on* state transition of the junction. In the case of electron doping, although the transmission increases slowly with carrier density, such a dramatic increase is absent.

In order to understand the asymmetry in Fig. 3, we select two typical doping cases and analyze in detail the composition of the band structures. These two points are indicated by the purple arrows in Fig. 3. One case is hole-doped, with a charge carrier density of 6.8×10^{12} cm^{-2} and high transmission. The other one is electron-doped, with charge carrier density of -10.8×10^{12} cm^{-2} and low transmission. For the selected hole-doped case, the band structure of the junction and the transmission function are plotted in Figs. 4(a) and 4(b). The red dots on bands indicate the degree to which MnPc states in the two leads are hybridized with those of NiPc. The radius of a red dot is proportional to $e^{-\lambda(\mathcal{N}_1 - \mathcal{N}_2)^2}$, where $\mathcal{N}_1$ and $\mathcal{N}_2$ are the projected density of states of MnPc and NiPc and λ is a positive constant. By examining panels (a) and (b) carefully, one can see that the high transmission in Fig. 4(b) is correlated with the size and density of red dots on the band structure in Fig. 4(a). When the hybridization between MnPc and NiPc states is strong, that is, the difference in the PDOS is small, the size of the red dot is large and the transmission is high. On the other hand, when the difference in the PDOS is large, the hybridization is weak and the red dot is small. Returning to Fig. 4(a), we see that some states at the Fermi energy are well hybridized. Consequently, the transmission at the Fermi energy is relatively large. One can also reveal such a relation by examining wave-vector-resolved transmission, as shown in Fig. 12 of Appendix C. The band structure and the transmission function are shown for the selected electron-doped case in Figs. 4(c) and 4(d). The analysis here is similar to that for the hole-doped case, except that the states at the Fermi energy are not well hybridized, and the transmission at the Fermi energy is relatively small.

Despite the low transmission at the Fermi energy for electron-doped cases, there is a transmission peak not far above the Fermi energy. However, due to relatively large density of states above the Fermi energy, it requires a high carrier density to bring down the transmission peak. Figure 5 shows the projected density of states (PDOS) of NiPc within the
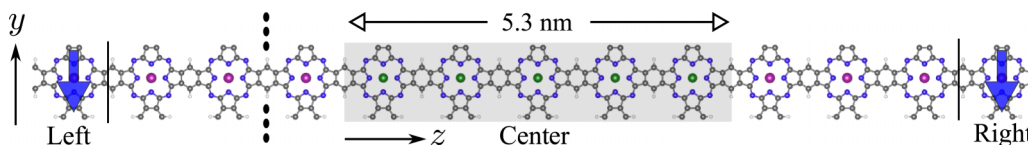

FIG. 2. Atomic structure of the MnPc-NiPc-MnPc junction with five NiPc unit cells in the center region. The black ellipses are to indicate the periodicity of the junction along the y direction. The vertical solid lines mark the boundaries between the center region and the leads. The blue arrows on the left and right sides indicate directions of local magnetization of MnPc. The grey shaded region in the middle is the NiPc channel.
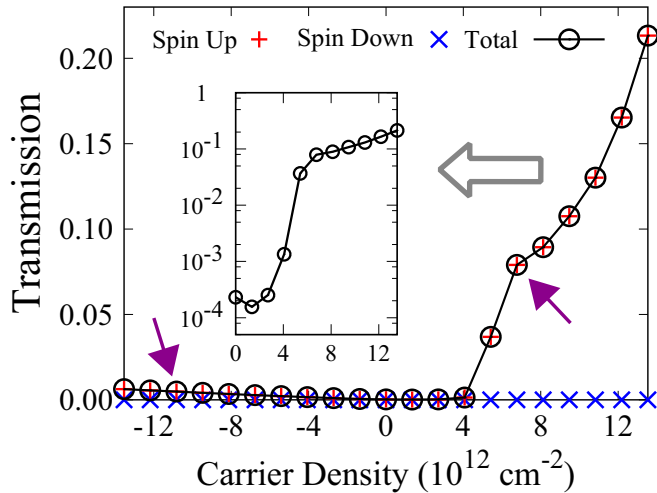
FIG. 3. Transmission at the Fermi energy versus charge carrier density for the MnPc-NiPc-MnPc junction with five NiPc unit cells in the center region. Different charge carrier density corresponds to different gate voltage. Positive/negative charge carrier density means hole/electron doping. The two purple arrows indicate two typical doping cases. The inset shows the total transmission on a logarithmic scale.

MnPc-NiPc-MnPc junction. It demonstrates that, for NiPc, the density of states of valence bands is higher than that of conduction bands. As a result, it takes more electrons than holes to achieve the same amount of shift of DOS in energy. This can also be shown by the spatially decomposed density of states, which is given in Fig. 13 of Appendix D. For comparison, the
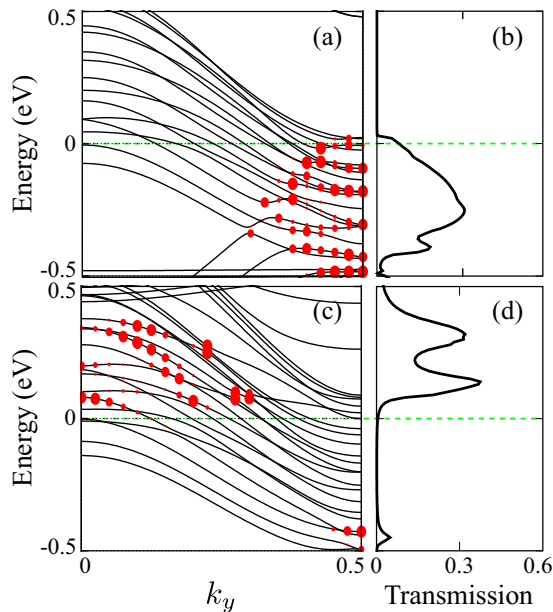

FIG. 4. (a) and (c) Band structure of the hole-doped/electron-doped MnPc-NiPc-MnPc junction with five NiPc unit cells in the center region. The size of the red dots represents the quality of hybridization between MnPc and NiPc states. (b) and (d) Transmission versus energy for the hole-doped/electron-doped junction. The Fermi energy is set to zero and is indicated by the green dashed line.
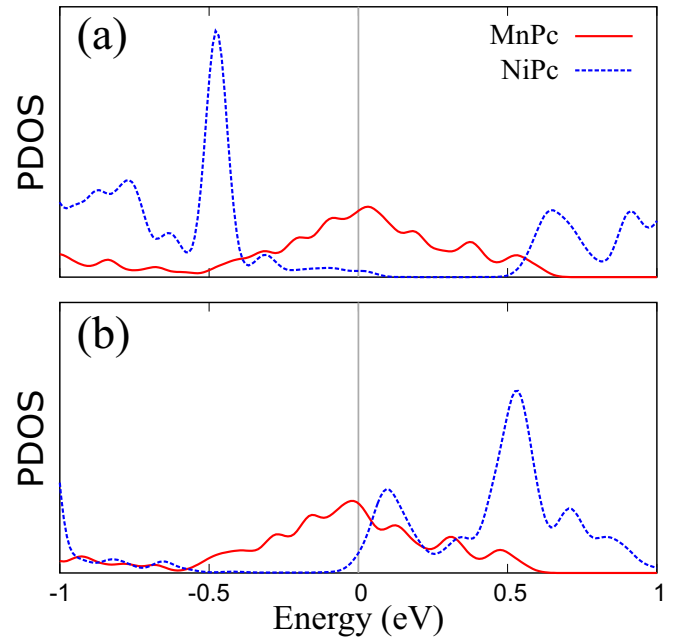

FIG. 5. Projected density of states (PDOS) for (a) the hole-doped case and (b) the electron-doped case. The red solid line represents the PDOS of the MnPc unit cell on the left. The blue dashed line represents the PDOS of the NiPc unit cell in the center.

PDOS for both the selected electron-doped and hole-doped cases indicated in Fig. 3 are given in the figure. Note that only the DOS for spin-up electrons is plotted here, since NiPc is nonmagnetic while MnPc is half-metallic with spin-up electrons being the majority ones.

To further understand the role of hybridization between MnPc and NiPc states, we examine the wave functions of two typical states. Isosurfaces of the modulus of the two wave functions are depicted in Figs. 6(a) and 6(b). Figure 6(a) represents a strongly hybridized state, for which the wave function is continuous through the whole junction; and Fig. 6(b) shows a poorly hybridized state, with a wave function with little support in the center region. Evidently, the spatially continuous state contributes more to the transmission than the disjoint one.

The results presented so far are for the MnPc-NiPc-MnPc junction with $N_{cell} = 5$ NiPc cells in the scattering region. For junctions with $N_{cell} = 1-4$ NiPc unit cells, trends in the transmission versus charge density are similar to those for $N_{cell} = 5$, especially for $N_{cell} = 3, 4$, as shown in Fig. 7. In this figure, the x-axis is set to net charge for comparison of transmission between junctions with different number of NiPc cells. For the junction with $N_{cell} = 5$, a net charge of $1\,e$ corresponds to carrier density of 6.8×10^{-12} cm^{-2}. As seen in Fig. 7, there is a dramatic increase in the transmission in the hole-doped case regardless of the number of NiPc unit cells. Such an increase in the transmission indicates that the valence band of NiPc starts to line up with the Fermi energy. The net charge at which the increase occurs does not change much with the number of NiPc unit cells. The reason behind this is as follows: first, holes are mainly doped into MnPc before the valence band of NiPc enters the Fermi energy. Second, the charge difference between the MnPc and NiPc regions largely
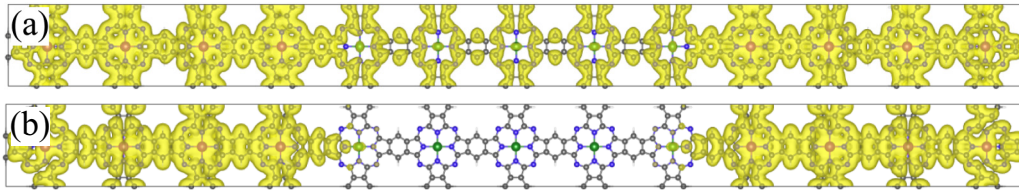
FIG. 6. Isosurface of the modulus of (a) a well and (b) a badly hybridized wave function of the junction. The contour threshold is 0.005 Å^{-3}.

determines the band alignment in the junction. From this, one can infer that it requires a certain net charge to bring the valence band of NiPc to the Fermi energy. In addition, the increase in the transmission is sharper when there are more NiPc unit cells. This is mainly because the transmission of the junction under zero gate voltage decays exponentially with the number of NiPc unit cells. We will elaborate on the N_{cell} dependence of the transmission coefficient later.

C. Magnetoresistance

The transport properties of MnPc-NiPc-MnPc junctions can also be tuned by external magnetic field. This is because a magnetic field can change the junction between parallel and anti-parallel magnetic configurations, and the magnetic configuration greatly affects electron transmission due to the half-metallic nature of MnPc. Let T_P and T_A be the transmissions for the junction in the parallel and antiparallel magnetic configurations. According to our calculations, T_P is seven orders of magnitude larger than T_A for MnPc-NiPc-MnPc junctions, as shown in Fig. 8. Defining a tunneling magnetoresistance (TMR) ratio as $\xi = |T_P - T_A|/(T_P + T_A)$, we see that ξ is nearly 100%. In this respect, the MnPc-NiPc-MnPc can act as a spin valve. The huge difference between T_P and T_A can be understood as follows. In the parallel magnetic configuration, the majority electrons in both left and right leads belong to the same spin channel. Thus the majority-spin channel is open for electron tunneling, while the minority-spin channel is blocked, and the total transmission is significantly large. However, in the antiparallel magnetic configuration, the majority electrons on left and right sides belong to different spin channels. As a result, both spin channels are blocked and the total transmission is zero. Note that the numerical value of T_A depends on the broadening parameter η of the Green's functions used for calculating electron transmission. However, as shown in Appendix E, T_A approaches zero as η tends to zero. (The TMR ratio is also likely to be decreased by spin-flip processes, but these are beyond the scope of this study.)

D. Length dependence of resistance

Finally, we discuss the dependence of transport properties of MnPc-NiPc-MnPc junctions on the length of the scattering region, that is, the length of the NiPc region. We consider here the parallel magnetic configuration. As the length increases, the total transmission at the Fermi energy decays exponentially, as shown in Fig. 8. The exponential decay is a signature of electron tunneling in the junction, and can be understood as follows. Since MnPc is metallic, there are propagating Bloch states at the Fermi energy in both left and right MnPc leads. In contrast, NiPc is semiconducting, and there are only decaying evanescent states at the Fermi energy, which lies within its band gap. Consequently, a scattering state in the MnPc-NiPc-MnPc junction at the Fermi energy is a superposition of propagating MnPc states and decaying NiPc states. Therefore NiPc works as a tunneling potential barrier for incoming electrons at the
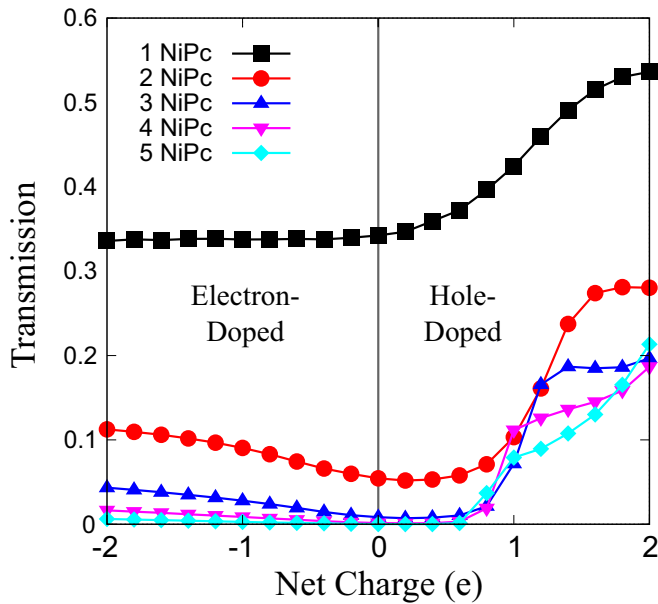

FIG. 7. Transmission at the Fermi energy vs net charge for MnPc-NiPc-MnPc junctions with different numbers of NiPc unit cells in the center.
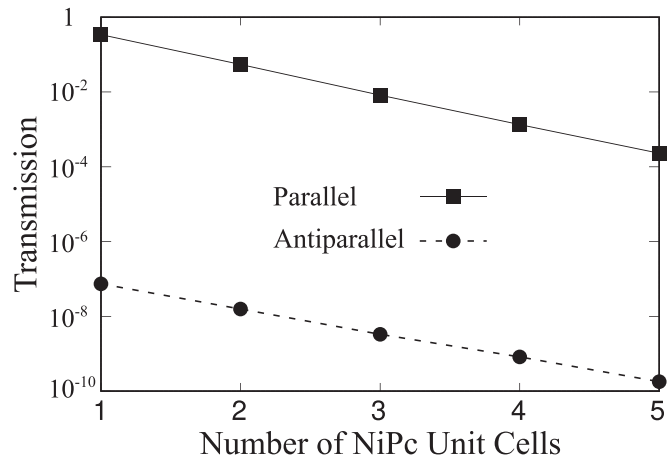

FIG. 8. Transmission of MnPc-NiPc-MnPc junctions in both parallel and antiparallel magnetic configurations. The transmission is evaluated at the Fermi energy.
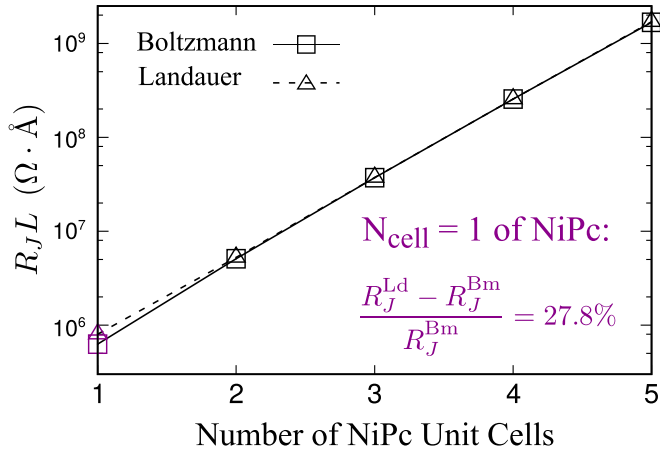
FIG. 9. Resistance vs the length of center region for MnPc-NiPc-MnPc junctions in the parallel magnetic configuration. The resistance was multiplied by the width of the junction.

Fermi energy, and the transmission decays exponentially with the barrier width. From the k-resolved transmission functions, we also calculate the resistance of the junction using both the Landauer Formula and the Boltzmann equation (see Fig. 9). For the junctions with two or more NiPc unit cells in the center region, both methods give similar results. For the junction with one NiPc unit cell, the transmission is about 0.34. In this case, Landauer formula overestimates the resistance by about 28% compared with Boltzmann equation, and the latter is more appropriate since the junction becomes conducting. A thorough discussion of this issue was given in Ref. [25].

IV. HIGHER-ORDER EFFECTS

Our results are based on the DFT PBE energy functional. Here we discuss possible effects of higher-level calculations, such as GGA+U and quantum Monte Carlo [11]. First, previous Monte Carlo simulations based on the Ising model have suggested that the Curie temperature (T_C) is about 150 K, which may imply that one may need low temperature to achieve the ferromagnetic state of MnPc and then the tunneling magnetoresistance. Second, higher-level calculations may bear a different band gap of NiPc, and as a result, the turn-on gate voltage may be different. However, the energy bands of MnPc and NiPc around the Fermi energy are dominated by p-orbitals that determine the transport properties of the MnPc-NiPc-MnPc junction under low level of electron/hole doping. Compared with d-orbital dominated energy bands, these p-orbital dominated bands are less likely to be affected by electron correlation. Therefore our results should be qualitatively valid with electron correlation considered.

V. CONCLUSION

In conclusion, we predict via first-principles calculations a strong on-off dependence of charge transport on applied gate field. The conducting channel is nearly 100% spin polarized, resulting in significant tunneling magnetoresistance. By examining the detailed electronic and magnetic structures and k-resolved transmission coefficients of two-dimensional metal

phthalocyanine junctions, we find that hybridization of states in the conducting leads (MnPc) and in the scattering region (NiPc) is the key factor determining on-off switching. In addition, our results show that electron transmission decays exponentially with the length of scattering region. When there are two or more NiPc unit cells in the center region, the resistance of the junction can be evaluated by either the Landauer formula or the Boltzmann equation. Finally, an asymmetry between hole doping and electron doping is observed. Due to a lack of hybridization (or mode matching between MnPc and NiPc states) in the window of applied gate field, the on-off switching shown in hole-doped scattering is absent in electron-doped systems. For additional ways of tuning the transport properties of MPc junctions, one may consider setting MnPc in the collinear antiferromagnetic state, see Figs. 14 and 15 of Appendix. Our work can stimulate and guide future experimental activities in the realization of such junctions.

APPENDIX A: ENERGY BANDS OF MnPc AND NiPc

The band structures of NiPc and MnPc are plotted in Figs. 10(a) and 10(b). It is clear from the band structure that NiPc is a nonmagnetic semiconductor, with each energy band being doubly degenerate due to spin. In contrast, MnPc is a ferromagnetic half-metal, with an energy gap around the Fermi energy for spin-down electrons but with two energy bands crossing the Fermi energy for spin-up electrons. In this paper, we refer the spin-up channel as the majority channel.
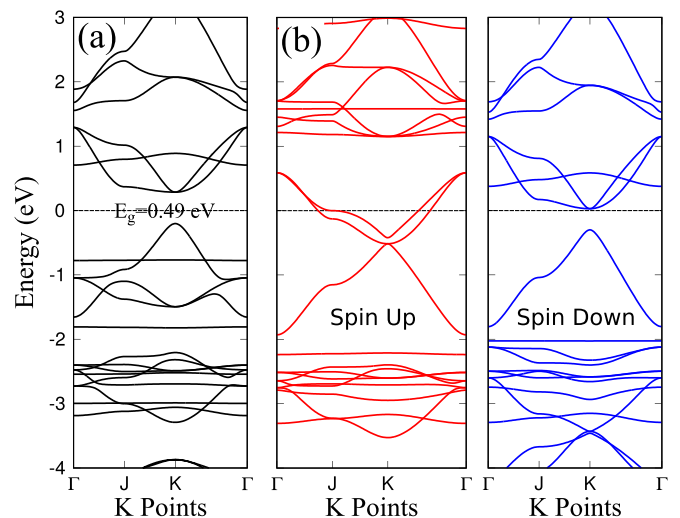

FIG. 10. Band structure of (a) NiPc (spin-up and spin-down degenerate) and (b) MnPc (spin up and spin down shown separately). NiPc is a nonmagnetic semiconductor while MnPc is a ferromagnetic half-metal.
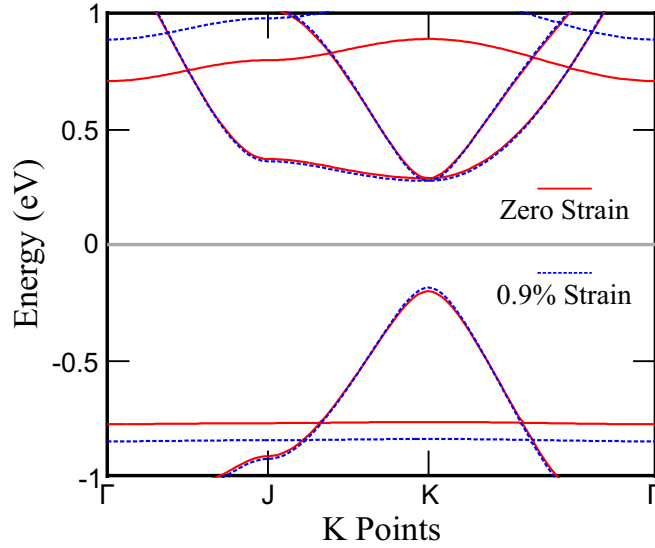
FIG. 11. Comparison of the band structures of NiPc with (blue dotted line) and without (red solid line) strain. The Fermi energy is set to zero, as indicated by the horizontal grey solid line.
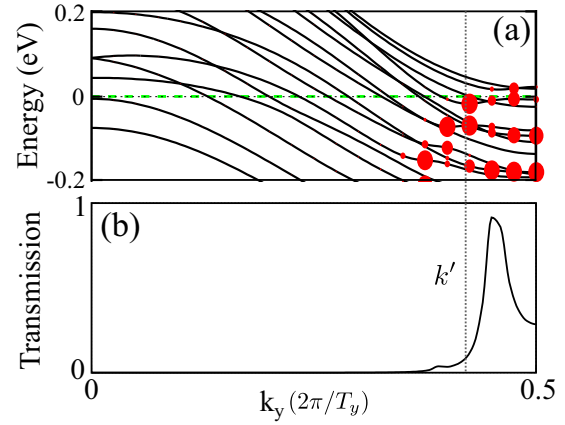

FIG. 12. (a) Band structure of the hole-doped MnPc-NiPc-MnPc junction with five NiPc unit cells in the center region. The size of the decorating red dots represents the quality of hybridization between MnPc and NiPc states. The Fermi energy is set to zero and is indicated by the green horizontal dotted line. (b) Transmission at the Fermi energy vs wave vector k_y. The vertical dotted line marks the wave vector k' where the transmission begins to rise steeply.

The calculated band gap for NiPc is about 0.49 eV, and the band gap for spin-down electrons of MnPc is 0.33 eV.

APPENDIX B: NiPc UNDER STRAIN

During the construction of the MnPc-NiPc-MnPc junction, unit cells of NiPc are stretched to match the lattice constant of MnPc. The equilibrium lattice constants of NiPc and MnPc are 10.56 and 10.66 Å, respectively, with a lattice mismatch of about 0.9%. In order to check whether an artificial strain on NiPc affects transport properties of the MnPc-NiPc-MnPc junctions, we calculate the band structure of NiPc before and after stretching. The results are plotted in Fig. 11, which shows that the energy bands within ± 0.5 eV around the Fermi energy are very nearly the same. Since only these energy bands are relevant to the transport properties presented in this work, effects due to the artificial strain are negligible.

APPENDIX C: k-RESOLVED TRANSMISSION

In the main text, we argue that well-hybridized states contribute more to the transmission. This can be also seen by examining individual states. We again plot the band structure of the hole-doped MnPc-NiPc-MnPc junction in Fig. 12(a) with curves accompanied by a red dot with a size representing the quality of hybridization between MnPc and NiPc states (see discussion of Fig. 4). In Fig. 12(b), we plot the transmission at the Fermi energy versus the wave vector k_y. There is a vertical dotted line marking a special wave vector denoted as k' such that to the left of k' the transmission is small but to the right of k' the transmission increases significantly. Comparing Fig. 12(a) with Fig. 12(b), we clearly see that the large transmission corresponds to well-hybridized states at the Fermi energy.

APPENDIX D: SPATIALLY DECOMPOSED DOS

In order to illustrate the effect of charge doping, in Fig. 13, we plot the spatially decomposed density of states (DOS) for the MnPc-NiPc-MnPc junction with 5 NiPc unit cells in the center region. The spatially decomposed DOS also helps us to understand the asymmetry in the dependence of electron transmission on carrier density, which is shown in Fig. 3 of the main text. In this figure, the x axis is the index label of MPc unit cells along the junction. There are 4 MnPc unit cells on both the left and right sides and five NiPc unit cells in the center region. The MPc unit cells with indexes of 1–4 belong to the left side; 5–9 belong to the center part; and 10–13 belong to the
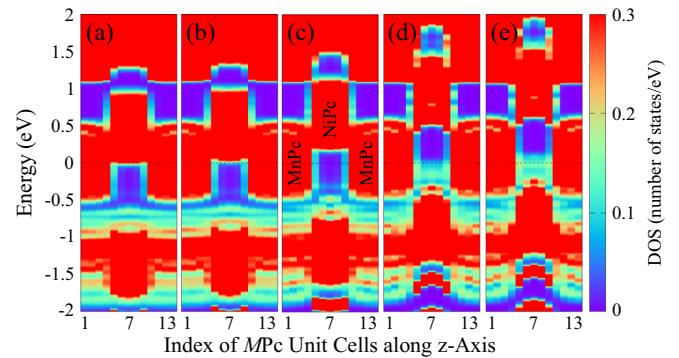

FIG. 13. Spatially decomposed density of state (DOS) for the MnPc-NiPc-NiPc junction, with five NiPc unit cells in the center region, under different charge carrier densities. (a)–(e) are for charge carrier densities of -10.8×10^{12}, -5.4×10^{12}, 0.0, 5.4×10^{12}, and 10.8×10^{12} cm^{-2}, respectively. The Fermi energy is set to zero, as indicated by the horizontal dotted line. Purple color means no states. As the color changes from purple to red, the density of states increases. The DOS is normalized such that the integration of total DOS up to Fermi energy equals the number of electrons in the simulated junction.
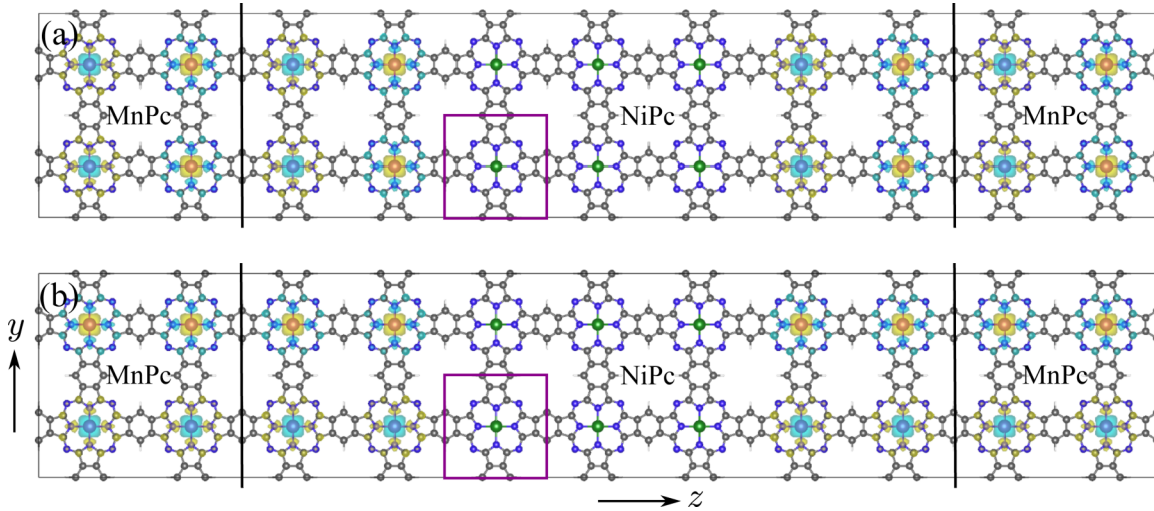
FIG. 14. Atomic structure and spin density of the MnPc-NiPc-MnPc junction with five NiPc unit cells in the center region. The isodensity thresholds are ± 0.002 Å^{-3}; cyan and yellow represent positive and negative values. The purple square indicates a unit cell of NiPc. In (a) the ferromagnetic coupling is along the y direction, and in (b) it is along the z direction.

right side. Figures 13(a)–13(e) are for different charge carrier densities, with (a) and (b) being electron doped and (d) and (e) being hole doped. Figure 13(c) shows the projected DOS for the neutral junction. In this figure, the red color around the Fermi energy on both left and right sides means that there are many states: MnPc is metallic. The purple region in the center indicates an energy gap around the Fermi energy: NiPc is a semiconductor. When the junction is doped with electrons, the energy bands of NiPc are shifted downwards in energy, along the vertical axis; eventually, the conduction bands will align with the Fermi energy as seen in Fig. 13(a). When electrons are removed from the junction, which is then doped with holes, and the energy bands of NiPc are shifted upwards along the energy axis; eventually the valence bands will align with the Fermi energy as seen in Fig. 13(e). However, the energy bands of NiPc are more easily shifted upwards than downwards. This is because the DOS of the valence bands is smaller than the DOS of the conduction bands, which can be clearly seen in the figure. As such, it requires more electrons than holes to achieve the same shift in energy.

TABLE I. Transmission and tunneling magnetoresistance (TMR) as a function of the Green's function broadening parameter η. T_P and T_A are the electron transmission for the MnPc-NiPc-MnPc junction with $N_{cell} = 5$ NiPc unit cells in the parallel or antiparallel magnetic configuration. TMR is defined as TMR $= (T_P - T_A)/(T_P + T_A)$.

η (eV)	T_P	T_A	$1 - $ TMR
1×10^{-5}	2.3×10^{-4}	1.8×10^{-9}	1.6×10^{-5}
1×10^{-6}	2.3×10^{-4}	1.8×10^{-10}	1.6×10^{-6}
1×10^{-7}	2.3×10^{-4}	1.8×10^{-11}	1.6×10^{-7}
1×10^{-8}	2.3×10^{-4}	1.8×10^{-12}	1.6×10^{-8}
1×10^{-9}	2.3×10^{-4}	1.8×10^{-13}	1.6×10^{-9}

APPENDIX E: DEPENDENCE ON BROADENING PARAMETER

Due to the half-metallic nature of MnPc, the electron transmission for the MnPc-NiPc-MnPc junction in the antiparallel magnetic configuration (T_A) should be zero, and as a result the tunneling magnetoresistance ratio (TMR) should be one. However, in our simulations T_A and TMR are not exactly zero or one. This is because we have applied a broadening parameter η in the Green's functions for calculating electron transmission, and the resulting transmissions and TMR depend on the value of η. This is unimportant for T_P; and T_A and TMR approach zero and one linearly as η tends to zero, as shown in Table I. For results in the main text, $\eta = 10^{-6}$ eV.
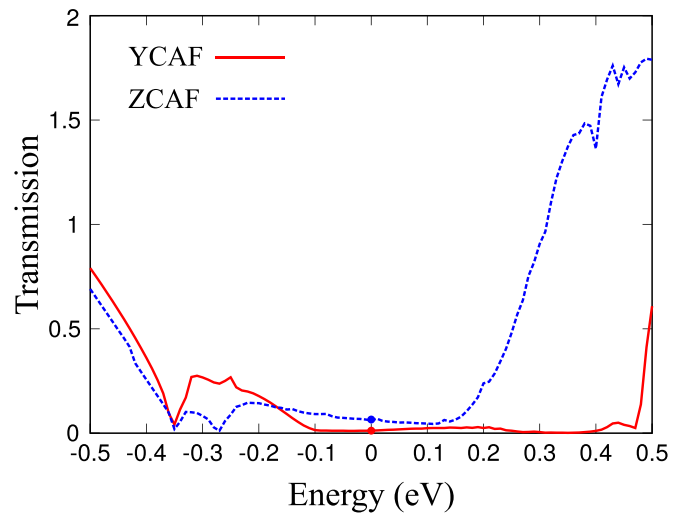

FIG. 15. Total transmission vs energy for the MnPc-NiPc-MnPc junction in YCAF and ZCAF magnetic states. The Fermi energy is set to zero.

APPENDIX F: ANTIFERROMAGNETIC ELECTRODES

According to our simulations, collinear antiferromagnetic (CAF) MnPc is metallic and thus can be used as the lead. It is then interesting to see what happens to the transport properties of the MnPc-NiPc-MnPc junction when we set MnPc to the CAF state. Figures 14(a) and 14(b) show two possible magnetic configurations of the MnPc-NiPc-MnPc junction with MnPc in the CAF state. The two configurations differ from each other in the orientation of the pattern of spin density; in Fig. 14(a) [Fig. 14(b)], the ferromagnetic coupling is along the y direction (z direction), and the corresponding magnetic configuration of the MnPc-NiPc-MnPc junction is denoted as YCAF (ZCAF). In both figures, the spin density is superposed over the atomic structure, where cyan and yellow represent positive and negative values beyond the density thresholds

$\pm 0.002 \, \text{Å}^{-3}$, respectively. We have calculated the transmission as a function of energy for the MnPc-NiPc-MnPc junction under zero gate voltage in both YCAF and ZCAF magnetic states. For both of these magnetic states, the transmissions of the junction for both spin-up and spin-down channels are the same. It is then sufficient to present the total transmission in Fig. 15. This figure shows that the trend of the transmission function versus energy is strongly affected by the YCAF or ZCAF magnetic configuration. The magnitude of the transmission around the Fermi energy also changes significantly when the magnetic configuration changes: the transmission at the Fermi energy for the MnPc-NiPc-MnPc junction in the ZCAF magnetic state, which is 0.061, is about five times larger than that for the junction in the YCAF magnetic state, 0.012.

[1] F. Schwierz, J. Pezoldta, and R. Granznera, Nanoscale **7**, 8261 (2015).

[2] M. Chhowalla, D. Jena, and H. Zhang, Nat. Rev. Mater. **1**, 16052 (2016).

[3] C. Tan, X. Cao, X.-J. Wu, Q. He, J. Yang, X. Zhang, J. Chen, W. Zhao, S. Han, G.-H. Nam, M. Sindoro, and H. Zhang, Chem. Rev. **117**, 6225 (2017).

[4] J. W. Colson and W. R. Dichtel, Nat. Chem. **5**, 453 (2013).

[5] C. Chakravarty, B. Mandal, and P. Sarkar, J. Phys. Chem. C **120**, 28307 (2016).

[6] J. Liu, Q. Sun, Y. Kawazoed, and P. Jenac, Phys. Chem. Chem. Phys. **18**, 8777 (2016).

[7] J. Zhou and Q. Sun, Nanoscale **6**, 328 (2014).

[8] J. Zhou, Q. Wang, Q. Sun, Y. Kawazoe, and P. Jena, J. Phys. Chem. Lett. **3**, 3109 (2012).

[9] M. Abel, S. Clair, O. Ourdjini, M. Mossoyan, and L. Porte, J. Am. Chem. Soc. **133**, 1203 (2011).

[10] M. Koudia and M. Abel, Chem. Commun. **50**, 8565 (2014).

[11] J. Zhou and Q. Sun, J. Am. Chem. Soc. **133**, 15113 (2011).

[12] P. Hohenberg and W. Kohn, Phys. Rev. **136**, B864 (1964).

[13] W. Kohn and L. J. Sham, Phys. Rev. **140**, A1133 (1965).

[14] G. Kresse and J. Hafner, Phys. Rev. B **47**, 558 (1993).

[15] G. Kresse and D. Joubert, Phys. Rev. B **59**, 1758 (1999).

[16] J. M. Solar, E. Artacho, J. D. Gale, A. García, J. Junquera, and P. Ordejón, and D. Sánchez-Portal, J. Phys: Condens. Matter **14**, 2745 (2002).

[17] P. E. Blöchl, Phys. Rev. B. **50**, 17953 (1994).

[18] J. P. Perdew, K. Burke, and M. Ernzerhof, Phys. Rev. Lett. **77**, 3865 (1996).

[19] H. J. Monkhorst and J. D. Pack, Phys. Rev. B **13**, 5188 (1976).

[20] M. Otani and O. Sugino, Phys. Rev. B **73**, 115407 (2006).

[21] Y.-P. Wang and H.-P. Cheng, Phys. Rev. B **91**, 245307 (2015).

[22] D. S. Fisher and P. A. Lee, Phys. Rev. B **23**, 6851 (1981).

[23] W. H. Butler, X.-G. Zhang, and J. M. MacLaren, J. Supercond. **13**, 221 (2000).

[24] Y.-P. Wang, J. N. Fry, and H.-P. Cheng, Phys. Rev. B **88**, 125428 (2013).

[25] Y.-P. Wang, X.-G. Zhang, J. N. Fry, and H.-P. Cheng, Phys. Rev. B **95**, 085303 (2017).